FAST COMMUNICATIONS

J. Appl. Cryst. (1998). **31**, 106–108

Visualization of inverted ferroelectric domains in $LiNbO_3$ by X-ray topography

P. REJMÁNKOVÁ,[a]* J. BARUCHEL,[a] P. MORETTI,[b] M. ARBORE,[c] M. FEJER[c] AND G. FOULON[b] *at* [a]*European Synchrotron Radiation Facility, BP 220, F-38043 Grenoble, France,* [b]*Laboratoire de Physico-Chimie des Matériaux Luminescents (URR CNRS 5620), Université Claude Bernard Lyon I, F-69622 Villeurbanne, France, and* [c]*Ginzton Laboratory, Stanford University, 94305 Stanford CA, USA. E-mail: rejma@esrf.fr*

(*Received 29 April 1997; accepted 4 September 1997*)

Abstract

A nondestructive method to visualize inverted ferroelectric domains in periodically poled $LiNbO_3$ by X-ray topography is reported. It is shown that, when an electric field is applied to the sample, a strong contrast revealing the inner structure of the domains can be observed, even in white-beam mode.

1. Introduction

Lithium niobate exhibits large optical nonlinearities and is widely used for electro-optic and acousto-optic applications as well as for frequency conversion. It has been suggested previously (Armstrong *et al.*, 1962) that, by changing of the sign of the nonlinear coefficient, every coherence length leads to efficient conversion by quasi-phasematching (QPM). An advantage of QPM is that it involves the highest nonlinear coefficient (d_{33} in the case of $LiNbO_3$). In ferroelectric materials, a way to achieve QPM is to reverse periodically the sign of the polarization.

A variety of methods for revealing domain reversal in $LiNbO_3$ crystals have been reported. The most widely used technique is chemical etching, followed by the direct observation of domains using an optical microscope, since the etching rate is faster for a negative $-z$ face than for a positive one (Nassau *et al.*, 1965). This is of course a destructive measurement. The use of transmission electron microscopy (Wicks & Lewis, 1968) or scanning electron microscopy (Houe & Townsend, 1995) allows visualization of the domains, but the electron beam itself may induce domain reversal. Pyroelectrically induced electron emission measurement (Kugel *et al.*, 1995) involves precise temperature control and a vacuum environment. A promising alternative method seems to be X-ray diffraction topography. Ferroelectric domains in lithium niobate are equivalent to inversion twins, which lead, under anomalous diffraction conditions, to a small but detectable X-ray diffracted intensity difference produced by differences in corresponding structure factors (Wallace, 1970; Vreeland & Speriosu, 1984). They also produce very faint distortion detected by multiple-crystal reflection X-ray topography (Hu *et al.*, 1996). To our knowledge, all X-ray topographic studies revealing ferroelectric domains in $LiNbO_3$ crystals have been performed recording projection topographs, when the three-dimensional sample is projected onto two-dimensional film. Information about the three-dimensional shape of inverted domains is then lost. In this work, using the section-topography technique in white-beam mode, which is a very simple set-up, and by applying an electric field along the c axis of the crystal, we have obtained strong image contrast corresponding to a 23 μm periodically inverted domain structure in $LiNbO_3$. A similar method has already been used to reveal hydrogen-implantation-related inverted domains in $LiNbO_3$ crystals (Rejmánková *et al.*, 1996).

2. Experimental

The periodically poled $LiNbO_3$ (PPLN) samples were fabricated by bulk electric field poling (Myers *et al.*, 1995). A 7.62 cm-diameter, 0.5 mm-thick, z-cut wafer of congruent $LiNbO_3$ from Crystal Technology was lithographically patterned on the $+z$ ($+c$) face with a 0.6 μm-thick, 23 μm-period grating of spin-on glass with 5 μm-wide openings. The wafer was then poled with an electric field of approximately 2×10^7 V m^{-1} at a regulated current of 23 mA until domain growth was self-terminated at approximately 100 ms, *i.e.* domain reversal was realized across the whole thickness of the sample. Subsequently, $5 \times 10 \times 0.5$ mm samples were cut from the wafer. Aluminium electrodes were evaporated onto the large-area surfaces, forming rectangles partially covering the surface area, schematically drawn in Fig. 1. A DC electric field was then applied along the c axis.

The diffraction section-topographic technique allows the visualization of deformations and misorientations in a 'virtual' slice of the crystal by restricting the incident beam width to ~20 μm as depicted in Fig. 1. This sometimes simplifies the interpretation because (as a first approximation) a nearly two-dimensional object is projected onto the two-dimensional film (Lang, 1958). The experiment was performed using synchrotron radiation at the ID19 ('topography') beamline at the ESRF. The section topographs were recorded as Laue patterns (white-beam diffraction topography in transmission) on Kodak Industrex SR films with a typical exposure time of about 20 s and a crystal-to-film distance of 25 cm. The small source size and the experimental configuration at the ID19 retain a good resolution with no image blurring, even for crystal-to-film distances greater than 20 cm (Barrett *et al.*, 1995). This allows the separation of images arising from regions inside a crystal misoriented by as little as 1 arcsecond. The spatial resolution is about 1 μm.

The z-cut sample was etched in the usual way (see, for example, Nassau *et al.*, 1965) and using the optical microscope in reflection mode the domain distribution was very distinctly observed. Fig. 2 shows a typical section topograph obtained after the sample etching with the slits set perpendicularly to the domain walls. The dots on the bottom of the section, which is an image of the exit surface of the sample, correspond to the strains on the crystal surface produced by the etching

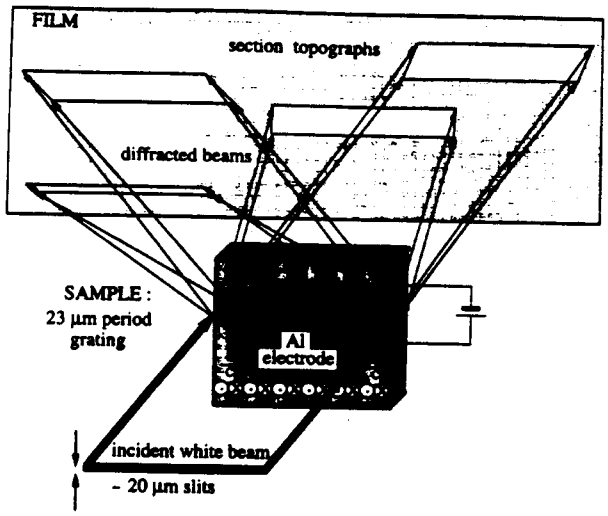

Fig. 1. Experimental set-up for the section topography in the white beam with a schematic drawing of the electroded $LiNbO_3$ z-cut sample. The latter has been periodically poled (23 μm period grating).

procedure, related to the inverted domains. Note this is in contrast to experience of the chemical etching procedure producing strain-free surfaces. The intersection of domains with the surface can therefore be well visualized, but no information can be extracted about the arrangement of the inverted domains in the bulk.

The investigated sample was then carefully polished using diamond paste up to the moment where there was no optical evidence of domain-inverted areas (magnification ~100). The subsequent X-ray white-beam projection topograph confirmed no obvious evidence of domain reversal. The polished sample was then electroded and a DC electric field of 4×10^6 V m^{-1} was applied along the c axis. Fig. 3 shows the $3\bar{1}1$ reflection section topographs without (Fig. 3a) and with (Fig. 3b) the applied field, recorded in the white-beam mode. Strong periodic black lines are observed in Fig. 3(b). Their period corresponds to the period of ferroelectric domain walls. The black lines appear to be parallel to the projection of the diffraction vector **g** on the film due to a geometrical projection effect. Note that a faint contrast is observed in Fig. 3(a), even in the absence of the electric field. This may suggest a phase-contrast imaging mechanism (Cloetens *et al.*, 1997). The contrast of the individual domains is greatly enhanced by the applied field and could correspond to the inverted

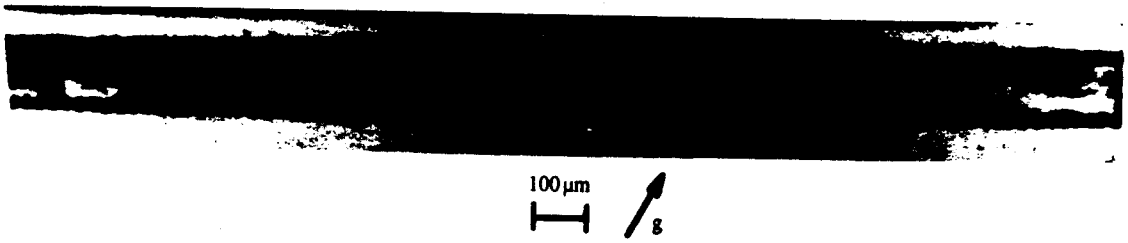

Fig. 2. Monochromatic section topograph of a periodically poled $LiNbO_3$ sample (z-cut, 0.5 mm thick): 309 reflection, $\lambda = 0.22$ Å, $\mu t \simeq 1$ (μ is the absorption coefficient and t the thickness of the sample; **g** is the projection of the diffraction vector on the film). The slits are set perpendicularly to the domain walls.

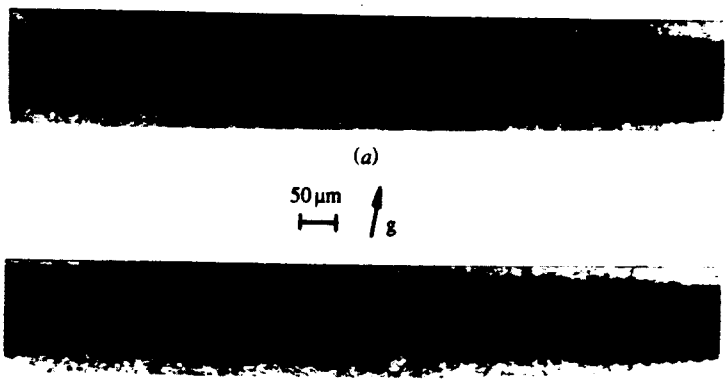

Fig. 3. White-beam section topograph of the same sample as in Fig. 2, but after polishing and electroding of the large-area surfaces: $3\bar{1}1$ reflection, $\lambda = 0.546$ Å, $\mu t \simeq 8.2$, with the main contribution of the $6\bar{2}2$ reflection, $\lambda = 0.273$ Å, $\mu t \simeq 1.3$. (a) $E = 0$, (b) $E = 4 \times 10^6$ V m^{-1} applied along the c axis. The slits are set perpendicularly to the domain walls.

piezoelectric distortion between domains produced by the field. The accurate explanation of the mechanism producing the observed contrast is under investigation.

3. Conclusions

The proposed method of revealing reversal of ferroelectric polarization using white-beam section topographs recorded when an electric field is applied to the investigated sample is very simple to use, and has the major advantage of topographic methods, *i.e.* it does not destroy or alter the crystal. This technique provides additional information about the domain inversion within the sample bulk. It should therefore be useful in investigating the domain-inversion mechanisms in ferroelectric crystals, depending on the inversion methods or conditions used, for second harmonic generation (SHG) applications. To our knowledge, this is the first unambiguous report on visualization of domain-inverted patterning for SHG applications inside a ferroelectric crystal.

References

Armstrong, J. A., Bloemberger, N., Ducuing, J. & Pershan, P. S. (1962). *Phys. Rev.* **127**, 1918–1939.

Barrett, R., Baruchel, J., Härtwig, J. & Zontone, F. (1995). *J. Phys. D*, **28**, A250–A255.

Cloetens, P., Guigay, J.-P., De Martino, C. & Baruchel, J. (1997). *Opt. Lett.* **22**. 1059–1061.

Houe, M. & Townsend, P. D. (1995). *Appl. Phys. Lett.* **66**, 2667–2669.

Hu, Z. W., Thomas, P. A. & Webjörn, J. (1996). *J. Appl. Cryst.* **29**, 279–284.

Kugel, V. D., Rosenman, G. & Shur, D. (1995). *J. Phys. D*, **28**, 2360–2364.

Lang, A. R. (1958). *J. Appl. Phys.* **29**, 597–598.

Myers, L. E., Eckardt, R. C., Fejer, M. M., Byer, R. L., Bosenberg, W. R. & Pierce, J. W. (1995). *J. Opt. Soc. Am.* **B12**, 2102–2116.

Nassau, K., Levinstein, H. J. & Lioacono, G. M. (1965). *Appl. Phys. Lett.* **6**, 228–229.

Rejmánková, P., Baruchel, J. & Moretti, P. (1996). *Physica B*, **226**, 293–303.

Vreeland, T. Jr & Speriosu, V. S. (1984). *Application of X-ray Topographic Methods to Materials Science*, edited by S. Weissmann, F. Balibar & J.-F. Petroff, pp. 501–509. New York and London: Plenum Press.

Wallace, C. A. (1970). *J. Appl. Cryst.* **3**, 546–547.

Wicks, B. J. & Lewis, M. H. (1968). *Phys. Status Solidi*, **26**, 571–576.